Journal of Visualization, Vol. 6, No. 4 (2003) 353-361

Application of PIV to Over-expanded Supersonic Flows: Possibilities and Limits

Ahn, K.*[1], Kim, J. H.*[1] and Yoon, Y.*[2]

*1 Graduate Research Assistant, School of Mechanical and Aerospace Engineering, Seoul National University, Shilim-dong, Kwanak-gu, Seoul, 151-742, Korea.
*2 Associate Professor, School of Mechanical and Aerospace Engineering, Seoul National University, Shilim-dong, Kwanak-gu, Seoul, 151-742, Korea.
E-mail: ybyoon@snu.ac.kr

Received 18 November 2002
Revised 15 May 2003

Abstract: Two-dimensional velocity distributions outside a Mach 2.0 supersonic nozzle have been investigated using a digital particle image velocimetry (PIV). Mean velocities, vorticity field and volume dilatation field were obtained from PIV images using 0.33 μm titanium dioxide (TiO_2) particle. The seeding particle of larger size, 1.4 μm TiO_2, was also used for the experimental comparison of velocity lag downstream of shock waves. The results have been compared and analyzed with schlieren photographs for the locations of shock waves and over-expanded shock structure to inspect possibilities and limits of a PIV technique to over-expanded supersonic flows. It is found that although the quantitative velocity measurement using PIV on over-expanded supersonic flows with large velocity and pressure gradients is limited, the locations of normal shock and oblique shock waves can be resolved by the axial/radial velocity fields, and over-expanded shock structure can be predicted by vorticity field and volume dilatation field which are acquired from the spatial differential of the velocity field.

Keywords: PIV, Over-expanded supersonic flows, Mean velocity, Vorticity, Volume dilatation

1. Introduction

For a long time, the supersonic flow outside the nozzle has received considerable attention, since it presents fundamental flow features existing in many practical engine nozzles, such as turbojets, ramjets, scramjets and rockets. However, our knowledge and experimental data of the flowfield have remained incomplete although understanding the dynamics of these flows is important. The primary reason is that the quantitative measurements of velocity, temperature and density were too difficult. For example, the physical probes, such as pressure tubes and hot wires, were used for the measurement of supersonic flows, but these techniques have the limitations that intrusive probes change the shock structure significantly.

Recently, non-intrusive optical techniques have been developed and successfully applied to supersonic flow. Particle image velocimetry (Höcker and Kompenhans, 1991; Krothapalli et al., 1994; Lawson et al., 1999; Yuceil et al., 2000), laser Doppler velocimetry (Clancy and Samimy, 1997) and Rayleigh scattering (Panda and Seasholtz, 1998) were utilized in measuring velocity and density, respectively.

Over the past decades, PIV has matured successfully from its development stage to a reliable

flow measurement technique as a non-intrusive two dimensional velocity measurement. Although PIV is well established, the application of the technique to transient high speed flow regimes has been limited. For example, optimized seeding levels in an interrogation region and appropriate seeding particles have limited the application of PIV to transient flow (Molezzi and Dutton, 1993). The requirement for optimized seeding levels was studied comprehensively by Adrian (1991).

In the over-expanded flow, the pressure at the nozzle exit is smaller than that of the ambient. Thus, oblique shock and normal shock waves are produced to overcome the pressure difference and then expansion waves develop so that the flow has large velocity and pressure gradients. The schlieren photograph was taken and then PIV technique was used to measure the velocity of flowfield.

In the present study, the objective is to correlate fluid characteristics obtained from a PIV technique with the structure of over-expanded supersonic flow. Therefore the fluid characteristics acquired from a PIV measurement, such as velocity distributions, vorticity field, volume dilatation field and shock wave locations were compared and analyzed with the schlieren photograph for suggesting the application possibilities and limits of a PIV technique to over-expanded supersonic flows.

2. Experimental Apparatus

2.1 Supersonic Nozzle Rig

The supersonic nozzle is designed to eject the jet flow of Mach 2.0. The axisymmetric nozzle is 10 mm in the exit diameter (d) and the expansion ratio between the exit area (A_e) and the throat area (A^*) is 1.687. Figure 1 shows the schematic of the supersonic nozzle. The settling chamber (d_c = 60 mm) is equipped with a thermocouple and a pressure transducer to measure air static conditions. Since the chamber area (A_c) is much larger than the throat area (A^*), it is assumed that stagnation conditions in the chamber are same as static conditions. Air flow rates can be supplied up to 50 g/s from a pressurized air tank and the pressure at the settling chamber can be increased up to 75 psig. In the present research, the pressure in the settling chamber is fixed at 60 psig in order to maintain over-expanded shock structures outside of the nozzle. And the temperature in the chamber is 296.4 K. A funnel type aerosol generator is used to obtain sufficient particle seeding density in an interrogation region.

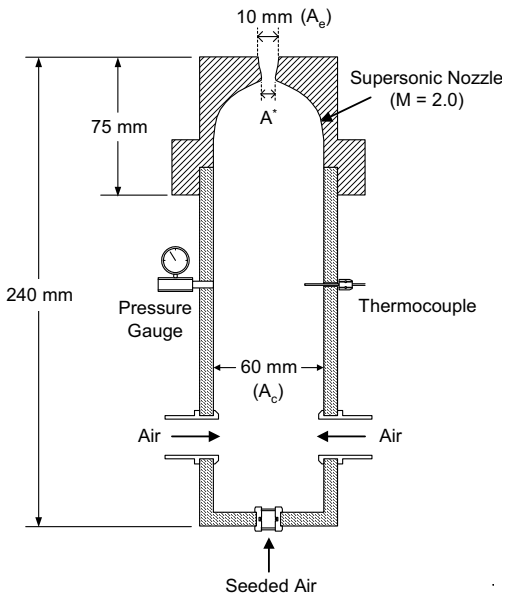

Fig. 1. Schematic of Mach 2.0 supersonic nozzle.

2.2 PIV System Set-up

Two 532 nm laser beams (2nd harmonic beam of Continuum PL-9050 YAG laser and 2nd harmonic beam of Spectra Physics GCR-170 YAG laser) are combined by a polarizer (532 nm, TP > 95.0 %, RS > 99.0 %, 56 deg), and then the combined beams are changed to sheet beams through a set of cylinderical lenses. Because the divergence of two laser beams is different, two convex lenses are used to make a focusing of two laser beams at the same location. For the alignment of two different laser light sheets, the laser beam reflecting from the polarizer was controlled carefully and the positions of two laser sheet beams were detected around 20 cm before and behind the focusing location, respectively. Since the recorded area (17 mm x 25.5 mm) in this experiment was small, the

thickness of two different laser sheet beams was almost the same. The power of the laser beam per pulse is 75 mJ and the duration of each pulse is 8 ns. The pulse separation between two laser beams is controlled by the delay generator (Stanford, DG535). The pulse separation is confirmed using a photo-diode and is fixed to 350 ns, which is equivalent to the 16 % length of an interrogation region when the velocity is 500 m/s.

Particles are seeded through another port of the nozzle chamber. It was not easy to maintain the uniform particle spatial density in this experiment because of high pressure in the chamber and a large velocity difference in the flowfield. However, on an average, particle pairs more than 10 existed in an interrogation window. Scattering intensities from seeding particles are recorded on a high resolution (3060 x 2036) Kodak digital CCD camera (DCS 460) equipped with a f/2.8 AF Micro Nikkor 105 mm lens and a tele-converter (KING 3x for Nikon). The F number of 105 mm lens is fixed to 5.6 throughout the experiments. The recorded area of scattering image is 17 mm x 25.5 mm. Velocity vectors are calculated by means of the FFT-based auto-correlation technique. The resolution of an interrogation region is 128 x 128 with a 50 % overlap, which is equivalent to the spatial size of 0.53 mm x 0.53 mm. The opening time of the camera shutter is controlled by the second delay generator so as to synchronize with the laser pulse. In the present research, all PIV measurements are automated through synchronization.

3. Experimental Considerations

Most laser Doppler anemometry depends on signals from particles suspended in the flow rather than on signals from the fluid itself (Durst et al., 1981). Similarly, PIV measures the velocity of tracer particles rather than the fluid. Thus, the measurement accuracy of PIV depends on the behavior of the seed particle. The motion of a particle in a fluid can be described by the following equation (Hinze, 1959) :

$$\frac{d\vec{u}_p}{dt} = \frac{18\mu_F}{d^2\rho_p}(\vec{u}_F - \vec{u}_P) - \frac{1}{\rho_p}\nabla p + \frac{1}{2}\frac{\rho_F}{\rho_P}\frac{\partial}{\partial t}(\vec{u}_F - \vec{u}_P) + \frac{9}{\pi d}\sqrt{\pi\rho_F\mu_F}\int_0^t \frac{\frac{\partial}{\partial t}(\vec{u}_F - \vec{u}_P)}{\sqrt{t-\tau}}d\tau - (\rho_F - \rho_P)\vec{g} \qquad (1)$$

In the above equation, the subscript F refers to properties of the fluid, P refers to properties of a particle and d is the diameter of a particle. The first forcing term models the viscous drag on the particle; the second term is due to pressure gradients within the flow field; the third term is an apparent mass effect; the fourth term is the Basset history integral; and the fifth term is due to the buoyancy of the particle.

Table 1. Seeding particles used in PIV and their relaxation time.

Particle size (d_p) [μm]	Material	Density [g/cm^3]	Relaxation time (τ_p) [μsec]
0.33	TiO_2	3.5 ~ 3.9	1.32
1.4	TiO_2	3.5 ~ 3.9	23.7

Researches on tracer particles have been conducted to study their scattering characteristics and flow tracking capability (Melling, 1997). In general, it is known that the light scattered by small particles is a function of the ratio of the refractive index of the particles to that of the surrounding medium, the particles' size, their shape and orientation, but the flow tracking capability of tracer particles is a function of their density and size mainly (Raffel et al., 1997). Hence, it is requisite to make a trade-off between decreasing the particle size to improve flow tracking and increasing the particle size to improve light scattering intensity. In the present research, we test the seeding particles of different diameters (d_p), such as 0.33 μm and 1.4 μm. Details of particles are listed in Table 1, where relaxation time (τ_p) is calculated by solving the equation of motion for the step response of a particle to a change in fluid velocity.

4. Results and Discussion

4.1 Schlieren Photograph

Schlieren photographs without particles and with particles were taken to look into the effect of seeding particles on the flow. Figure 2 (a) shows a schlieren photograph of the flow without seeding particles and Fig. 2 (b) shows a schlieren photograph of the flow with seeding particles, where the origins of radial direction (*r/d*) and axial direction (*x/d*) are located at the centerline and nozzle exit, respectively. The schlieren photograph with seeding particles (Fig. 2 (a)) looks unclean compared to the schlieren photograph without seeding particles (Fig. 2 (b)). However, the over-expanded shock structure and normal/oblique shock locations in the near field are not much changed by seeding particles for PIV measurements. Figure 2 (c) explains the structure of shock and expansion waves. At the exit of the nozzle, the shock front begins obliquely as a conical surface. And then, the shock front is cut off by a "Mach shock disc (normal shock)" perpendicular to the axis. Behind the incident and Mach shock front, a reflected shock front and a discontinuity surface (jet boundary) develop. After a reflected shock front meets jet boundary, reflected expansion waves develop. Due to viscosity at the jet boundary, this periodic jet pattern is eventually blurred and dies out (Courant and Friedrichs, 1948). The normal shock location and the 2nd reflected shock wave location at the centerline (*r/d* = 0) are 3 mm (*x/d* = 0.3) and 14.5 mm (*x/d* = 1.45) from the exit, respectively (Fig. 2 (b)).

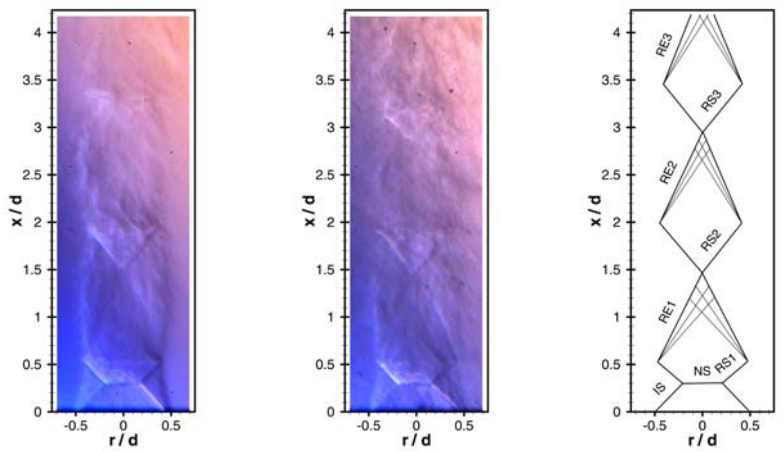

(a) (b) (c)

Fig. 2. Schlieren photographs and sketch of shock waves (IS : incident shock, NS : normal shock, RS1 : 1st reflected shock, RE1 : 1st reflected expansion wave): (a) without particles, (b) with particles and (c) sketch of shock waves (*d* is the nozzle exit diameter, 10 mm).

4.2 Mean Velocity Distribution

Figure 3 (a) shows the original PIV image obtained using 0.33 μm TiO_2 particles from the nozzle with a stagnation plenum pressure of P_0 = 60 psig and a stagnation plenum temperature of T_0 = 296.4 K. Figure 3 (b) shows the velocity vector plot, where an axial velocity of 400 m/s is subtracted from the original PIV data to show vividly the difference between the flow before and behind the normal shock and the spatial resolution is 0.53 x 0.53 mm. Mean velocities were calculated from 300 instantaneous PIV images. The area adjacent to the nozzle exit could not be processed perfectly and had a large bad vector rate because of excess scattering from the out surface of the nozzle. PIV data showed a significant overestimated velocity around jet boundary because of the size of the interrogation window (1.06 mm x 1.06 mm) and the velocity lag of particles.

Figure 4 shows the axial and radial velocity distributions obtained using 0.33 μm TiO_2 particles outside the nozzle. The flow behind the nozzle is axisymmetric so that the two-dimensional

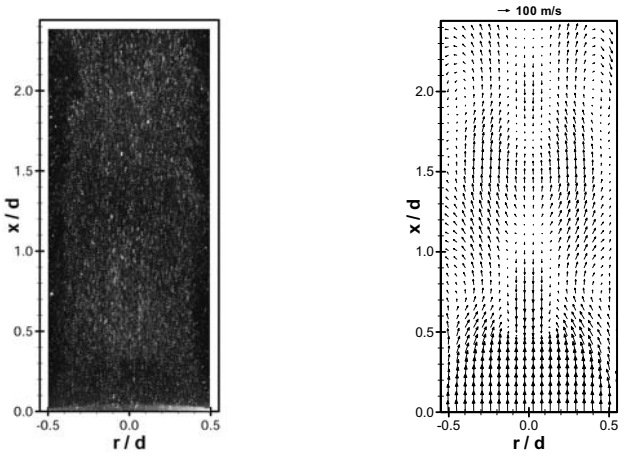

Fig. 3. PIV sample image and velocity vector plot: (a) sample image recorded with 0.33 μm TiO_2 particles and (b) velocity plot subtracted by 400 m/s in the axial direction.

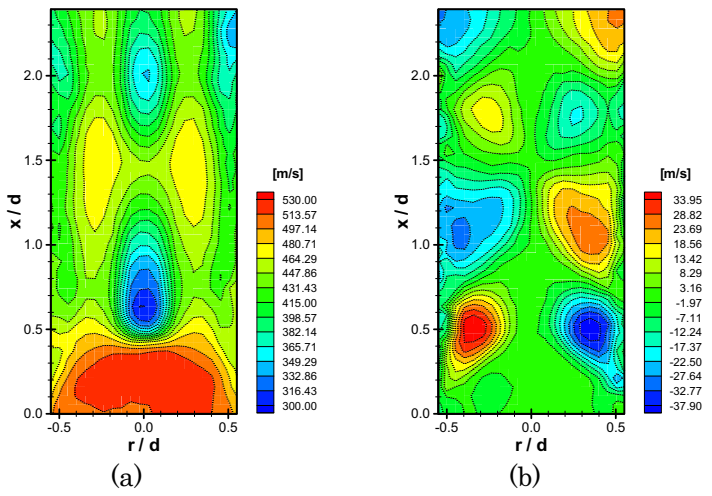

Fig. 4. Velocity distributions of axial and radial velocity components: (a) axial velocity distribution and (b) radial velocity distribution.

axial and radial profiles are symmetric to the centerline (r/d = 0). Axial flow velocity behind the normal shock is smaller than that behind the oblique shock. The flow moves inward through an incident shock wave and moves outward through the 1st reflected oblique shock wave. The flow due to the jet boundary and expansion waves moves outward and inward again, and then moves outward through the 2nd reflected oblique shock wave. This is also shown in Fig. 3 (b). Because the flow through the incident shock wave mixes the flow through the normal shock, the subsonic flow behind the normal shock changes into the supersonic flow again within a few mm downstream. The normal shock location, the oblique shock location, expansion waves and shock waves can be predicted approximately from the axial velocity and the radial velocity profiles.

Figure 5 presents the velocity profiles at the centerline for PIV measurements. Because the particles have a much larger density than air, the tracer particles cannot follow air flow immediately so that a velocity lag is found in the region where an abrupt change in the velocity exists. In the PIV result using 0.33 μm particle, supersonic flow of 520 m/s adjacent to the nozzle (denoted as circle A in Fig. 5 (a)) is decelerated to subsonic flow of 300 m/s after crossing a normal shock (circle B). And then

subsonic flow of 300 m/s is accelerated to supersonic (circle C) flow crossing expansion waves and mixed with supersonic flow behind incident/reflected shock waves. In the PIV result the normal shock location is determined as the next point of a maximum axial velocity point, because an interrogation region includes shock length.

As previously proposed by Lawson et al. (1999), PIV can resolve the shock and normal shock locations in one interrogation region length. If we define the shock position according to Lawson et al. (1999), the position of the normal shock acquired from PIV measurements is x = 3.2 mm (x/d = 0.32), which is almost the same as the value (x = 3 mm) acquired by the schlieren photograph. The difference is within one spatial resolution (0.53 mm). And, the position of the 2nd reflected shock acquired from PIV is x = 14.8 mm (x/d = 1.48), which is also almost the same as the value (x = 14.5) obtained by the schlieren photograph. The PIV result using 1.4 μm particle shows a similar pattern as that using 0.33 μm particle. However, with the increase of particle size, the tracking capabilities of particles decreased; the amplitude of velocity oscillation decreased and the delay of velocity lag increased. According to Melling (1997), TiO_2 particle with a diameter of 0.45 μm has a ten times larger frequency response in turbulent flow than TiO_2 particle with a diameter of 1.44 μm.

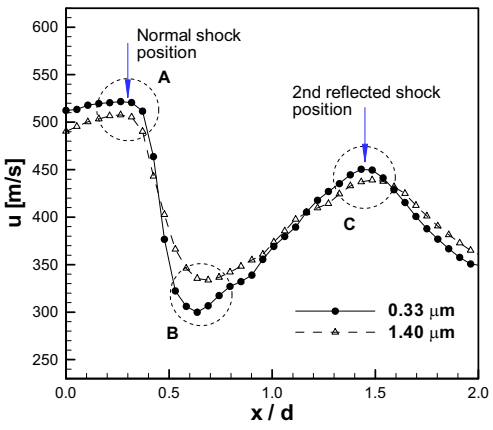

Fig. 5. Velocity profile along the centerline obtained by CFD result and PIV (Arrows indicate the locations of the shock waves by schlieren photographs).

The flow velocity after the normal shock must be reduced abruptly from 520m/s to a subsonic velocity of 200 m/s (White, 1994). However, because of the limit in tracking capability, the PIV velocity (particle velocity) falls only to 300 m/s and is delayed by 3 mm. As particles are accelerated again by increasing flow velocity around the circle B, particle velocity ceases falling and increases, and then reaches a peak value around the circle C. After reaching the peak value, particles are decelerated by the flow with some delay.

It is interesting that although quadrupling the particle diameter reduces viscous drag by a factor of 16, these results do not show a significant difference. The reason is believed to be due to the agglomeration of solid particles and the remaining four terms of equation (1). In this experiment with large velocity and pressure gradients, the pressure gradient's effect on the particles cannot be neglected, as the difference between particle velocity and fluid velocity is smaller. The actual size of particles can not be determined easily as long as their sizes have not been measured in-situ and the size might vary due to practical aspects like agglomeration. According to Melling (1997), the particles dispersed into the gas stream are normally several times larger than the nominal particle size of the powder in the bed because of coagulation which depends on the humidity of the gas and the moisture content of the powder, and on the rate of flow through the bed. In this experiment, it is believed that the agglomeration of particles could not be removed because particles with high velocity passed through the throat of the nozzle and the number concentration of particles increased rapidly around the throat of the nozzle.

Since PIV is based on a statistical measurement of the displacement using the correlation between two interrogation windows, a displacement gradient across the window is likely to result in biased data since not all of the particle images present in the first interrogation window will also be present in the second interrogation window, even if the mean particle image displacement is accounted for (Raffel et al., 1997). It is known that as the interrogation window size or the displacement gradient increases, the measurement uncertainty increases. In this experiment, over-expanded supersonic flows have a large velocity gradient inside shock region. As a percentage of the maximum velocity, absolute errors are calculated approximately as 6 % inside shock region and 2 % outside shock region, respectively. These values are similar to the result of Lawson et al. (1999)

which had 5.1 % error inside shock region and 2.7 % error outside shock region for 15 % particle image displacement of the interrogation window. From these results, the quantitative velocity measurement using PIV on over-expanded supersonic flows is believed to be limited.

4.3 Differential Quantities of the Velocity Field

It is not easy to analyze fluid characteristics through only the velocity fields. Thus the velocity field is transformed into the vorticity field (ω_θ) and the volume dilatation field (η), which indicate rotation and deformation of a fluid element, to show fluid characteristics of the over-expanded shock structure. Figure 6 shows the vorticity field and the volume dilatation field. These values can be calculated from PIV data as follows :

$$\omega_\theta = \frac{\partial V_x}{\partial r} - \frac{\partial V_r}{\partial x} \tag{2}$$

$$\eta = \varepsilon_{xx} + \varepsilon_{rr} + \varepsilon_{\theta\theta} = \frac{\partial V_x}{\partial x} + \frac{1}{r}\frac{\partial r V_r}{\partial r} + \frac{1}{r}\frac{\partial V_\theta}{\partial \theta} = \frac{\partial V_x}{\partial x} + \frac{1}{r}\frac{\partial r V_r}{\partial r} = \frac{\partial V_x}{\partial x} + \frac{\partial V_r}{\partial r} + \frac{V_r}{r} \tag{3}$$

where $\varepsilon_{\theta\theta}$ can be assumed to be zero since the jet flow is axisymmetric.

The high vorticity regions at the outer edges of the nozzle define the shear layers and as mixing takes place this outer shear layer grows in the axial direction (Yuceil et al., 2000). Around *x/d* = 0.6, a set of high vorticity regions are found to exist. The flow through the normal shock wave is subsonic, while the flow through oblique shock wave is still supersonic. Therefore, these high vorticity regions are generated by high turbulent mixing due to velocity difference. Another high vorticity regions are also found around *x/d* = 1.9 downstream of 2nd reflected shock wave. These results show a similar pattern as the results of Yuceil et al. (2000), which were obtained from highly underexpanded jets.

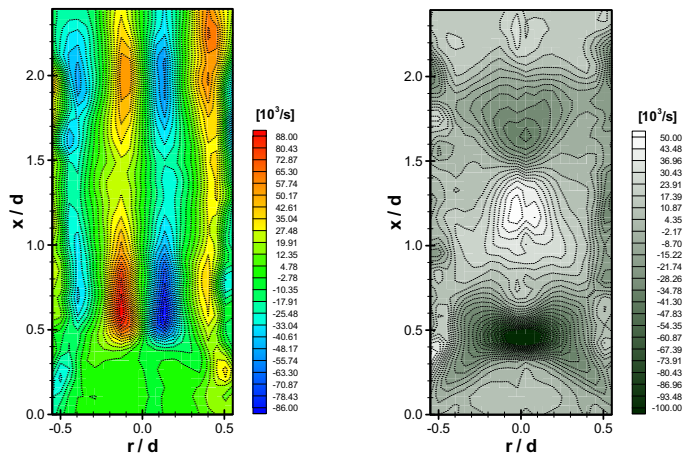

Fig. 6. Vorticity and volume dilatation distribution: (a) vorticity field and (b) volume dilatation field.

Figure 6 (b) shows the volume dilatation field which is acquired using equation (3). Since the nozzle is axisymmetric and the measurement plane (*r-x* plane) is on the center of the nozzle exit, $\varepsilon_{\theta\theta}$ can be assumed to be zero. Comparing Fig. 6 (b) with Fig. 2 (c), it is found that the flow has negative volume dilatation values (dark region) through normal shock wave and oblique shock waves, and has positive volume dilatation values (white region) through expansion waves. Since negative values indicate the compression of flows and positive values indicate the expansion of flows from equation (3), and their absolute values mean the degree of compression or expansion of a fluid element, it can

be said that the volume dilatation field acquired by PIV results is in good agreement with the schlieren photograph and predict over-expanded shock structure in terms of the degree of compression and expansion.

The centerline distributions of the volume dilatation are presented in Fig. 7. The values, which go below 0, are found around x/d = 0.3 and x/d = 1.45 from the nozzle exit. These locations correspond exactly to the locations of normal shock and 2nd reflected shock waves from the schlieren photograph. Thus the value of the volume dilatation can be a good indicator of shock and expansion waves. From these results, it can be inferred that the expansion waves are located around x/d = 0.64 and x/d = 2.00.

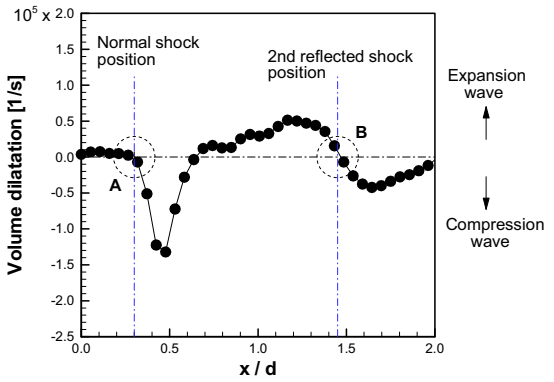

Fig. 7. Volume dilatation along the centerline (r/d = 0) (Dashdot lines indicate the locations of the shock waves by schlieren photographs).

5. Conclusion

The application of particle image velocimetry to over-expanded supersonic flows has been accomplished. The two-dimensional velocity distributions outside a Mach 2.0 supersonic nozzle have been measured using different sizes of seeding particle, such as 0.33 μm TiO_2 and 1.4 μm TiO_2, for the measurements of the velocity lag downstream of shock waves. The results, such as the velocity distribution, shock locations and over-expanded shock structure, have been obtained and compared with the schlieren photograph.

The over-expanded shock structure and normal/oblique shock locations in the near field of the nozzle are not altered seriously by seeding particles for PIV measurements. The sudden change in velocity after the normal shock wave and the oblique shock waves can not be measured exactly, because this technique depends on the behavior of particles; the increase of a seeding particle diameter gives rise to the increase of a velocity lag due to the inertia effect of the particle and the pressure gradient's effect on the particle in this experiment can not be neglected as the difference between particle velocity and fluid velocity is smaller.

However, the locations of shock waves can be resolved in one interrogation region length by PIV results, such as axial/radial velocity fields and volume dilatation field. Turbulent mixing regions between the subsonic flow through normal shock wave and the supersonic flow through oblique shock wave can be confirmed by the vorticity distribution. Also, the shock and expansion waves of the over-expanded shock structure can be predicted by the volume dilatation distribution.

Acknowledgments

This work was supported by a grant (No. 98-0200-04-01-3) from the Basic Research program of KOSEF (Korea Science & Engineering Foundation) and a grant (No. M1-0104-00-0058) from the National Research Laboratory program of the KISTEP (Korea Institute S & T Evaluation and Planning). This support is gratefully acknowledged.

References

Adrian, R. J., Particle-Imaging Techniques for Experimental Fluid Mechanics, Annual Review of Fluid Mechanics, 23 (1991), 261-304.

Clancy, P. S. and Samimy, M., Two-Component Planar Doppler Velocimetry in High Speed Flows, AIAA Journal, 35 (1997), 1729-1738.

Courant, R. and Friedrichs, K. O., Supersonic Flow and Shock Waves, Interscience Publishers, New York, (1948).

Durst, F., Melling, A. and Whitelaw, J. H., Principle and Practice of Laser-Doppler Anemometry (Second edition), (1981),

Academic Press.
Hinze, J. O., Turbulence: An Introduction to its Mechanism and Theory, McGraw-Hill, New York, (1959).
Höcker, R. and Kompenhans, J., Application of Particle Image Velocimetry to Transonic Flows, in Application of Laser Techniques to Fluid Mechanics, ed. R. J. Adrian et al., Springer Verlag, 416-434, (1991).
Krothapalli, A., Whishart, L. M. and Lourenco, L. M., Nearfield Structure of a Supersonic Jet: On-line PIV Study, Proc. 7th International Symp. Appl. Laser. Tech. Fluid Mech., Lisbon, Portugal, 2 (1994), 26.
Lawson, N. J., Page, G. J., Halliwell, N. A. and Coupland, J. M., Application of Particle Image Velocimetry to a Small-Scale de Laval Nozzle, AIAA Journal, 37 (1999), 798-804.
Melling, A., Tracer Particles and Seeding for Particle Image Velocimetry, Measurement Science & Technology, 8 (1997), 1406-1416.
Molezzi, M. J. and Dutton, J. C., Application of Particle Image Velocimetry in High Speed Separated Flows, AIAA Journal, 31 (1993), 438-446.
Panda, J. and Seasholtz, R. G., Density Measurement in Underexpanded Supersonic Jets Using Rayleigh Scattering, AIAA Paper 98-0281, (1998).
Raffel, M., Willert, C. E. and Kompenhans, J., Particle Image Velocimetry: A Practical Guide, (1997), Springer.
White, F. M., Fluid Mechanics (Third edition), (1994), McGraw-Hill, Singapore.
Yuceil, K. B., Otugen, M. V. and Arik, E., Underexpanded Sonic Jets: A PIV Study, 10th International Symp. on Application of Laser Techniques to Fluid Mechanics, Lisbon Portugal, July 10-13 (2000).

Author Profiles

Kyubok Ahn: He is a Ph.D. candidate at School of Mechanical and Aerospace Engineering in Seoul National University. He received his MS degree at School of Mechanical and Aerospace Engineering in 2001 from the same University. His research interests are laser diagnostics, such as PIV and PLIF, aerodynamics in a ramjet combustor and transverse liquid injection in subsonic crossflows.

Ji-Ho Kim: He received his Ph.D. degree and MS degree at school of Mechanical & Aerospace Engineering in Seoul National University in 2003 and 1998, respectively. Currently, he is a senior research engineer of Hyundai Motor Company. His research interests are laser diagnostics, such as simultaneous PIV and PLIF, bluff-body stabilized supersonic flame, and numerical simulation for model scramjet engine.

Youngbin Yoon: He received his MS degree at School of Mechanical and Aerospace Engineering in 1987 from Seoul National University and his Ph. D. degree at Department of Aerospace Engineering in 1994 from University of Michigan. After obtaining Ph.D. he worked as a researcher in University of California, Davis. And then he joined Seoul National University and currently is an associate professor. His research interests are visualization, laser diagnostics, supersonic combustion, turbulent diffusion flames and liquid rocket injectors.